UV Absorption Measurements of Nitric Oxide Compared to Probe Sampling Data for Measurements in a Turbine Engine Exhaust at Simulated Altitude Conditions

R. P. Howard
Sverdrup Technology, Inc., AEDC Group
Arnold Engineering Development Center
Arnold Air Force Base, TN 37389-9013

Presented at
AGARD
90th Propulsion & Energetics Panel (PEP)
"Advanced Non-Intrusive Instrumentation for Propulsion Engines"
October 20-24, 1997
Brussels, Belgium

UV ABSORPTION MEASUREMENTS OF NITRIC OXIDE COMPARED TO PROBE SAMPLING DATA FOR MEASUREMENTS IN A TURBINE ENGINE EXHAUST AT SIMULATED ALTITUDE CONDITIONS*

R. P. Howard
Sverdrup Technology, Inc., AEDC Group
Arnold Engineering Development Center
Arnold Air Force Base, TN 37389-9013

ABSTRACT

Nitric oxide measurements were conducted in the exhaust of a turbofan engine at simulated altitude conditions in a ground-level test cell using both optical nonintrusive and conventional gas sampling techniques. NO-UV absorption measurements, using both resonance and continuum lamps, were made through several chords of the exhaust flow near the nozzle exit plane as a part of a larger effort to characterize aircraft exhaust constituents over a wide range of steady-state engine operating conditions. This paper describes the NO-UV absorption measurements and compares radial profiles of NO concentrations and emission indices with measurements obtained using conventional gas sampling and tunable diode laser infrared absorption.

INTRODUCTION

The NASA Atmospheric Effects of Aviation Program requires characterization of aircraft emissions including trace constituents to adequately assess and predict the impact of current and future fleets on atmospheric chemistry. The first of a series of NASA measurement programs[1] in ground-based engine test cells was performed at the Arnold Engineering Development Center (AEDC) at simulated altitude conditions ranging from sea-level-static to 15.3 km. The test article engine design and operation parameters were representative of a commercial-type bypass engine with an annual combustor, operating with aviation fuel. The engine was operated over a range of combustor temperatures and pressures at each of several simulated altitudes shown in Fig. 1, to provide NASA with parametric data for insight into exhaust emission variations as a function of combustor parameters and altitude at standard-day conditions. Measurement systems applied directly to the exhaust flow field are illustrated in Fig. 2. Techniques utilized for measurements of nitric oxide (NO) concentrations were conventional extractive sampling using a multipoint cruciform probe rake assembly, spectral UV resonance and continuum absorption applied over multiple lines of sight, and spectral infrared single line-of-sight absorption utilizing a tunable diode laser. This paper details the NO-UV absorption techniques, directly compares the results to probe-sampled data, and compares the resulting NO emission indices including the tunable diode laser results to show agreement within the respective error limits of each measurement technique.

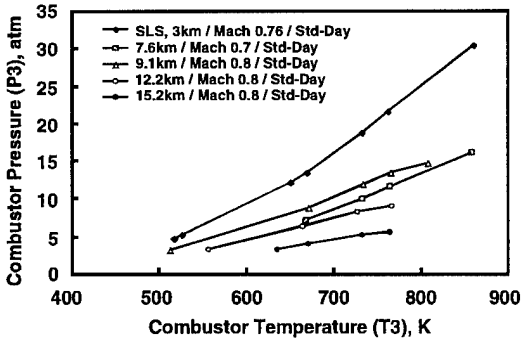

Fig. 1. Combustor pressure versus temperature for all test conditions.

Spectral interrogation of nitric oxide (NO) resonance electronic (A←X) transitions using ultraviolet (UV) absorption allows determination of NO density and, under appropriate conditions, thermodynamic state. NO-UV absorption techniques were developed in the 1970's[2] for measurements of low NO concentrations in gas turbine combustors and engines. These techniques were later modified and enhanced in response to new requirements for nonintrusive quantitative measurements in high-enthalpy test facility flows,[3,4] exhausts of liquid rockets (unpublished), and automobile exhausts.[5] The hardware was made robust and more reliable using spectrometer focal plane array detectors, fiber optics, and pulse-start power supplies for the resonance lamps. The line-by-line radiative transfer model, previously limited to the NO gamma (0,0) band, was extended to include the (0,1) band and thus allowed simultaneous determination of NO number density and ground electronic state-vibrational population distribution (reported as ground-state vibrational temperature) in many of the aforementioned applications. Renewed interest in the effects of turbine-powered aircraft on atmospheric chemistry has again prompted exhaust characterization studies and new requirements for quantitative measurements of NO concentrations in turbine engine exhaust.

PROBE AND SAMPLING SYSTEMS

Exhaust samples were extracted using a multipoint cruciform rake assembly located near the engine nozzle exit plane with the versatility of single point and multiple probe average sampling. The rake illustrated schematically in Fig. 2 consists of two bars mounted perpendicularly (horizontally and vertically) with each completely spanning the exhaust flow field and beyond. Individual probe sampling allowed spatial mapping of the exhaust core, bypass, and intermediate mixed flow regimes as well as the region surrounding the exhaust which was found to contain low amounts of recirculated exhaust constituents. The horizontal bar also contained alternating Mach number/flow angularity (MFA) and stagnation temperature

* The research reported herein was performed by the Arnold Engineering Development Center (AEDC), Air Force Materiel Command. Work and analysis for this research were performed by personnel of Sverdrup Technology, Inc., AEDC Group, technical services contractor for AEDC. Further reproduction is authorized to satisfy needs of the U. S. Government. **Approved for public release; distribution unlimited.**

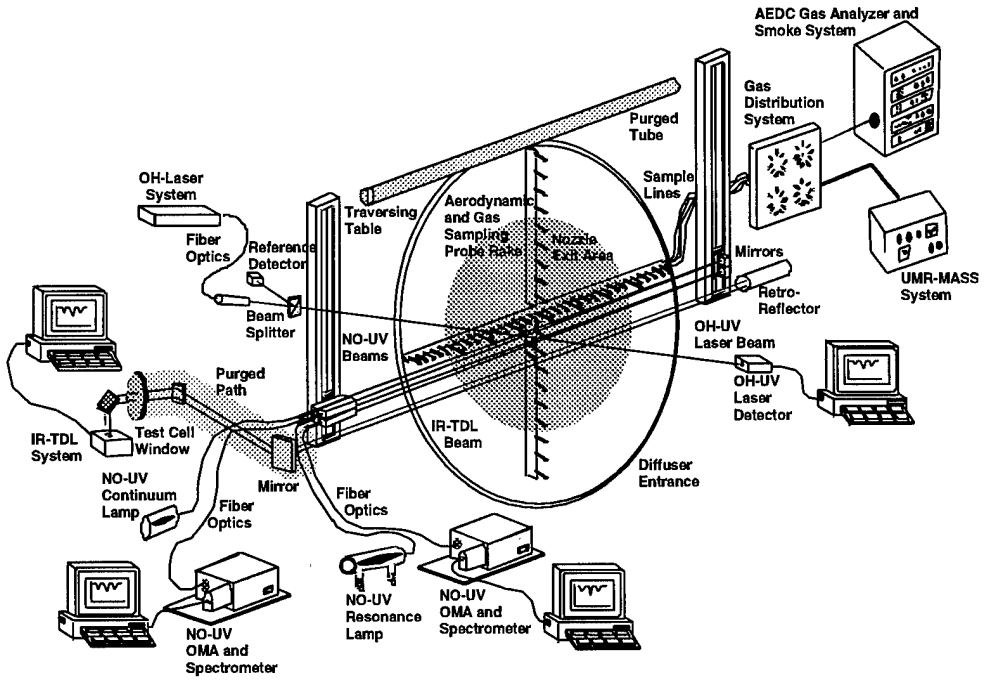

Fig. 2. Illustration of the turbine engine exhaust emissions measurement systems.

probes for determination of static temperature, static pressure, and gas velocity distributions required for analysis of optical data to yield species concentrations and mass fluxes. Construction and design details of each probe type are given in Ref. 1.

Gas samples collected by the rake positioned 12 cm downstream of the nozzle exit plane were passed through heated lines to a heated sample distribution system that allowed any combination of probe samples to be directed to the gas analyzer systems. As necessary during the test period, a stainless steel metal bellows pump was valved in line between the sample distribution system and gas analyzers to raise the sample pressure slightly above atmospheric pressure, a requirement for gas analyzer operation.

A suite of analyzers were used to measure concentrations of gaseous constituents which are reported in parts per million by volume (ppmv). A chemiluminescence analyzer was used to measure concentrations of NO after the sample was passed through a gas sample dryer. The emission index (EI) for NO, defined as mass of constituent per 1,000 pounds of fuel, was calculated according to Ref. 6 and reported as the NO_2 equivalent.

UV ABSORPTION INSTRUMENTATION

The resonance and continuum absorption system components were similar except for radiation sources. The system and technique similarities make it convenient to describe system components, data acquisition, and data analysis for both systems simultaneously while pointing out differences only as necessary. Primary components per measurement system, resonance or continuum, included a lamp, a lamp shutter with an electronic controller, two fiber-optic cables, collimating and focusing optics, a grating spectrometer, an optical multichannel analyzer (OMA®) detector system with a computerized controller, and a personal computer for data acquisition and storage. The systems shared stepper motor-driven slide tables for traversing the optical beams across the exhaust flow field.

The resonance lamp, a source of NO resonant radiation, was a dc excited capillary discharge tube operated at 12 ma using a 5,000-V power supply with a 220-kΩ ballast resistance. A gaseous mixture of argon:nitrogen:oxygen, at a 12:3:1 ratio by volume, was flowed through the lamp tube while maintaining a static pressure of 10 torr. The capillary discharge tube was water cooled to tap water temperatures. Resonance lamp intensity characterization is discussed in the following section. The continuum system lamp was a constant voltage, 100 w, water-cooled deuterium lamp.

Each detector system consisted of a 0.32-m Czerny Turner spectrometer with a variable-width entrance slit, a 2,400 groove/mm grating (used in first order) and an EG&G Princeton Applied Research Model 1421-B silicon diode array detector. Each detector was UV enhanced and intensified over the full 1,024 pixel elements. A detector and detector controller (Model 1461) are referred to as the OMA. The spectral range for the resonance absorption system was 214 to 245 nm with a 0.029-nm-per-detector-element spectral dispersion and 0.16-nm spectral resolution (full-width-half-maximum). Measured normalized instrument response functions representative of single array elements for both the resonance absorption and continuum absorption systems are presented in Fig. 3. Differences are due primarily to spectral resolution differences for the two systems.

The configuration and reported spectral region for the UV continuum absorption measurement deserves explanation. This measurement system had been configured and installed with intentions of measuring OH resonance absorption near 300 nm. During an engine checkout run, this system failed to detect OH absorption. A spectrally scanned UV laser system, successfully installed for measurements of OH, freed this system to be reconfigured for measurements of NO using a spectral continuum

lamp. The optical fibers, excellent for measurements at 300 nm, had a steep attenuation gradient in the region of NO absorption near 226 nm. Lamp radiation saturated the detector in the region of the (0,1) absorption band for detector integration times allowing a sufficient signal-to-noise ratio at the (0,0) band absorption region. Therefore, the less important (0,1) spectral region was moved off the detector to avoid detector damage. Also, the fiber attenuation was too great for meaningful measurements at wavelengths below the (0,0) band. Measurements were performed effectively from 222 to 228 nm with a 0.029-nm-per-detector-element spectral dispersion and 0.21-nm spectral resolution (full-width-half-maximum). As mentioned earlier, measured normalized instrument response functions representative of single array elements are presented in Fig. 3.

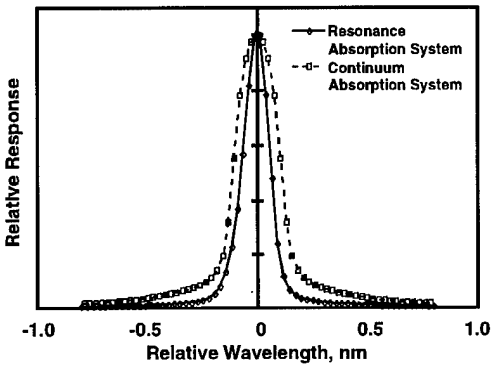

Fig. 3. Instrument response functions relative to the array element center wavelength.

RADIATIVE TRANSFER MODEL AND RELATED PARAMETERS

A computer model based on the theoretical line-by-line radiative transfer for the NO gamma (0,0) band was used to determine the NO number density from spectral absorption measurements. The theoretical physics of NO molecular absorption, details of the model, and extension of the model from earlier work can be found in the references.[2,3,7,8] A brief overview is presented here to describe and document model parameters used for analysis of the present data. Basically, the fractional lamp radiation within the wavelength interval $\Delta\lambda$ transmitted through a medium of length, L, is given by the equation of radiative transfer,

$$\tau_{\Delta\lambda} = \frac{\sum_j \int_{\Delta\lambda} \left(I_C + I_{\lambda_i^o}(\lambda) \right) e^{-\sum_i \int_L k_{\lambda i}(\lambda) dL} g(\lambda) d\lambda}{\sum_j \int_{\Delta\lambda} \left(I_C + I_{\lambda_i^o}(\lambda) \right) g(\lambda) d\lambda} \quad (1)$$

where

$g(\lambda)$ =spectral instrument response function,

$k_{\lambda i}(\lambda)$ =molecular absorption transition (line),

$I_{\lambda_i^o}(\lambda)$ =relative intensity of a resonance lamp transition,

I_C =Lamp radiation factor, modeled as continuum radiation.

The interval $\Delta\lambda$ is limited by the spectral extent of $g(\lambda)$, the spectral response for an individual element of the linear array detector given in Fig. 3 for the current measurements. Absorption in the test media is modeled by molecular absorption transitions, $k_{\lambda i}(\lambda)$, which are described by Voigt line profiles that allow for pressure or collision broadening. The summation over i includes all transitions of the NO gamma (0,0) or (0,1) band contributing to absorption within $\Delta\lambda$. The absorption coefficient is a function of the static temperature, static pressure, directed velocity line center shifts (Doppler shifts), line center pressure shift parameter, broadening parameter (discussed later), and NO number density along the measurement path, L. For a single homogeneous path, the flow-field parameters are input to the model, and the NO number density is varied until the calculated [Eq. (1)] and corresponding measured transmittances agree. Calculations were compared to maximum absorption at the second bandhead, 226.23 nm or 236.3 nm, respectively, for the (0,0) and (0,1) bands using the resonance absorption technique and 226.18 nm for the (0,0) band using the continuum absorption technique. As discussed earlier, the (0,1) band was not measured with the continuum absorption system.

Absorption media line center shifts with respect to the fixed lamp radiation line positions are important to the NO densities derived from the model. Two shift mechanisms are modeled. However, Doppler shifts were negligible for these measurements due to small exhaust flow velocity components in the direction of the source beam. Collision-induced shifts were modeled according to the collisional shift parameter, $\delta = -0.18*(295/T)^{0.56}$, as quantified in Ref. 9. Here "P" is static pressure in atmospheres and "T" is static temperature in Kelvin.

The resonance lamp radiates several lines within, or contributing to, the spectral interval $\Delta\lambda$ of Eq. (1). Line intensities, $I_{\lambda_i^o}(\lambda)$, are modeled by Doppler profiles broadened to 950 K. The relative lamp line intensities were measured and characterized according the upper state population distribution shown in Fig. 4. Results for the (0,0) and (0,1) bands were similar as expected, since the upper states are common to both bands. The lamp emits low-level radiation (I_C) in addition to gamma band radiation. This radiation was not directly quantifiable from lamp characterization measurements, but was modeled as constant continuum radiation, I_C, over the spectral range $\Delta\lambda$, [Eq. (1)], with excellent results.

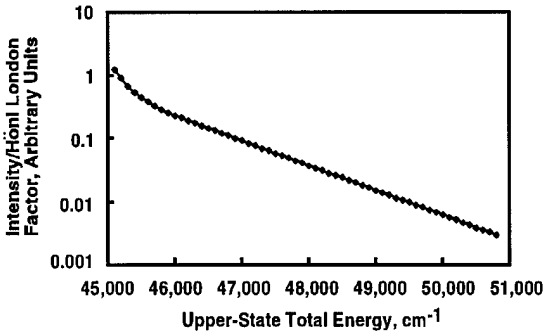

Fig. 4. Reasonance lamp line intensity distribution.

The lamp radiation for the continuum absorption technique was modeled as a simple spectral constant, achieved in Eq. (1) by setting, $I_{\lambda_i^o}(\lambda)$, to zero and I_C to some arbitrary constant value.

For the resonance technique, the molecular broadening parameter, $a' = C*P/T^n$, and I_C have been treated as instrument-dependent calibration factors[3] selected to minimize differences

in calculated and measured transmittances at controlled laboratory conditions. Here, "C" is referred to as the broadening constant and "n" the temperature dependency exponent. The broadening parameter, $a' = 31800*P/T^{1.5}$, was reported in 1981[7] but did not include a low-level lamp radiation factor, I_C. When this technique was reinstated in the late 1980's using the intensified array detector and a modified electronic lamp power supply, the radiative transfer model required a factor $I_C = 22$ (relative to the arbitrary scale used in Fig. 4) to accurately match laboratory-measured transmittances down to 0.2. Without I_C, the model predicted transmittances accurately down to about 0.8 but underpredicted at lower transmittances with increasing deviation. Since I_C had little effect on transmittance calculations above 0.8, a' was determined from a wide range of laboratory conditions (P, T, and NO number density) approximately independent of I_C. The results for a' were consistent with the 1981 reported value. Also, a two parameter nonlinear least-squares fit to all the laboratory data with the temperature exponent, n, fixed at 1.5 gave $I_C \approx 22$ and, again, a' consistent with the 1981 values. The study concluded that radiative transfer model calculations and laboratory data were in excellent agreement over the full range of laboratory conditions for $I_C = 22$ and $a' = 31800*P/T^{1.5}$. In recent years, the broadening parameters for individual lines have been measured directly[9] and reported as $a' = 6927*P/T^{1.25}$. It is both important and gratifying that this agrees extremely well with $a' = 31800*P/T^{1.5}$. Using the Ref. 9 value in the model, $I_C = 22$ was still the best fit value. Relative to the Fig. 4 lamp characterization values, I_C and a' were approximately equivalent for both the (0,0) and (0,1) bands.

The instrument-dependent code calibration parameter, a', was determined independently for the continuum absorption system using continuum lamp transmittance measurements over a similar range of laboratory measurements. For the continuum absorption system, the broadening constant C = 23,250 provided the best overall fit to laboratory data with the temperature-dependency exponent, n, fixed at 1.5.

A radial inversion scheme, referred to as an onion peel technique, coupled to the line-by-line radiative transfer model, was used to determine radial profiles of NO number density from a series of line-of-sight (LOS) measurements at several radial locations during a steady-state test condition, as illustrated in Fig. 5. The flow field was modeled as concentric "homogeneous" zones, one for each LOS measurement. The NO density in the outer zone was determined using the outermost LOS measurement. Stepping inwardly, a new zone NO density was determined for each successive measurement. The static temperature and static pressure along the optical path were inferred from probe measurements as discussed in Ref. 1. Probe measurements at similar radial positions on opposite sides of the plume centerline were averaged and radial symmetry was assumed. Measurements of ambient test cell static temperature were assigned to positions beyond the lip of the diffuser and ambient pressure assigned to radial positions just beyond the nozzle exit radius, Re = 30 cm. Radial distance was normalized to the nozzle exit radius so that the extent of the engine exhaust was R/Re = 1.0 or a little beyond, depending upon exhaust expansion for each test condition. The probe measurement grid was sparse; thus, interpolation was required to determine the path average static temperature, static pressure, and axial flow velocities for each homogeneous zone along each LOS measurement path. Averages were area weighted over the width of the optical beam within respective zones. Figure 6 shows representative plots of zone-averaged temperature, pressure, and the axial component of velocity for an LOS through the center of the exhaust. Values inferred from probe measurements used to determine the zone averages are superimposed on the plot. These data were

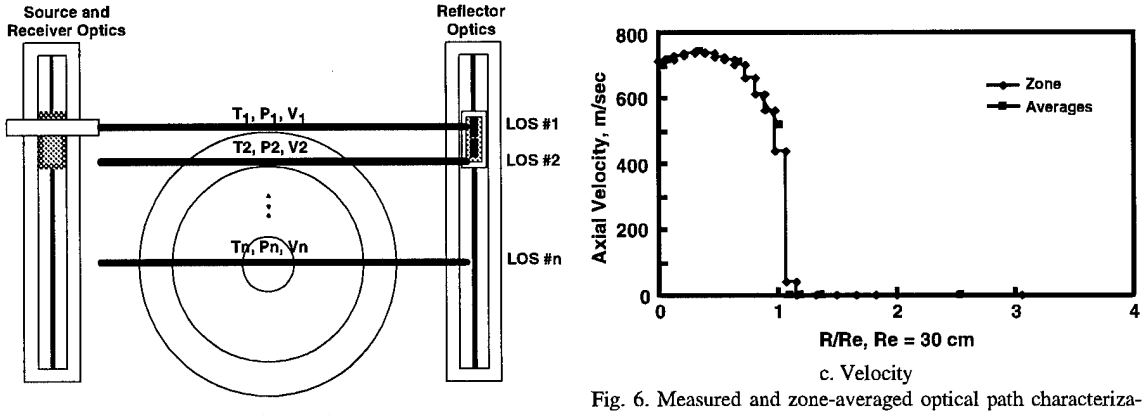

Fig. 5. Measurements through homogeneous zones.

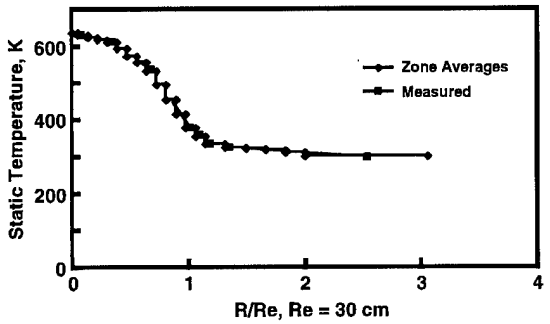

a. Static temperature

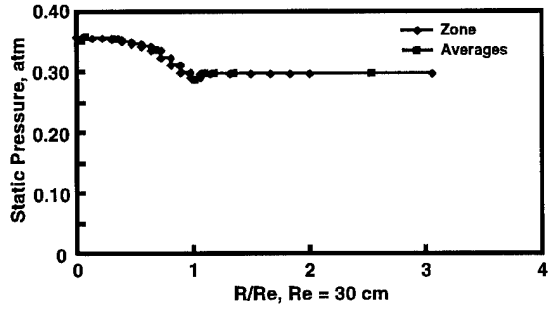

b. Static pressure

c. Velocity

Fig. 6. Measured and zone-averaged optical path characterization profiles.

acquired for the steady-state engine test condition described by the combustor inlet temperature 733 K at 9.15 km altitude. The zone path segments are obvious in the plot with approximately 2.54-cm (1.0-in.) lengths from the center to just outside the exhaust flow field and about 5.08 cm segment lengths in the test cell gas recirculation region. Zones beyond the nozzle exit radius represent measurements through the test cell air which contained small quantities of recirculated exhaust gases.

TEST CELL INSTALLATION AND MEASUREMENTS

The placement of the NO-UV instrumentation and optical beam paths relative to other measurement and facility components in the test cell are illustrated in Fig. 2. The lamp radiation was transmitted through a 400-μm-diam, 9-m-long, fused silica fiber to a collimating lens mounted onto a traversing table near the engine exhaust. The radiation was imaged through the exhaust to an aluminum-surfaced mirror mounted on a second traversing table and reflected back through the exhaust to a second lens-fiber combination also mounted on the first traversing table. The beam diameter was approximately 2 cm. The transmitted and reflected beams were within the first 12 cm downstream of the nozzle exit plane. The resonance lamp beam was 6.35 cm above that of the continuum lamp. The reflected radiation was transmitted to the entrance slit of the spectral detector system. All optical lenses and fibers were made of UV-grade fused silica.

In addition to measurements through the exhaust, LOS measurements were made at several positions outside the exhaust flow field to quantify and account for the presence of NO in the test cell due to recirculated exhaust gases. Low levels of NO over rather long paths can have a significant effect on the optical measurements. A tube purged with dry nitrogen mounted at the top of the diffuser allowed measurements of reference spectra for each set of measurements across the exhaust flow field. For data analysis, cylindrical symmetry was assumed for recirculated gas components surrounding the exhaust flow field.

The slide tables traversed the collimated beam across the flow field in a plane parallel to the nozzle exit plane, as illustrated in Figs. 2 and 5. Each set of traversed data for the resonance absorption system consisted of measurements through the purged path at the top of the diffuser (with and without the shutter closed) and measurements at fixed radial positions from R = 70 to 36 cm in 5.08-cm increments and from R = 36 to 0 cm in 2.54-cm increments. The nozzle exit radius was 30 cm. The set of continuum absorption measurement positions were offset about 6.35 cm below the resonance absorption measurements, except for measurements through the purged tube. A traversing system output voltage (high during movement and low while stationary) was monitored by each OMA system for posttest determination of spectra acquired while the tables were in motion.

During earlier engine checkout runs, measurements made while the lamp was shuttered were found to be indistinguishable from background signal levels. Therefore, acquisition time was significantly reduced by not shuttering the lamp except at the centerline position. These centerline data were used to verify that exhaust radiation levels were negligible for each engine condition. It is also significant that measurements were not affected by test cell lighting. Background levels, measured with the lamp shuttered, were almost entirely integrated detector noise as discussed in OMA operation manuals.

DATA REDUCTION

Spectral lamp transmission measurements, $I_T(\lambda_i)$, at a particular LOS (radial) position were reduced to spectral transmittance according to the equation

$$\tau_i = \frac{I_T(\lambda_i) - I_e(\lambda_i)}{I_0(\lambda_i) - I_b(\lambda_i)} \approx \frac{I_T(\lambda_i) - I_b(\lambda_i)}{I_0(\lambda_i) - I_b(\lambda_i)} \qquad (2)$$

where λ_i denotes the spectral center of the i^{th} element of the detector array. $I_0(\lambda_i)$ and $I_b(\lambda_i)$, respectively, are measurements of lamp reference and background at the purged path location. As mentioned earlier, measurement of lamp-shuttered signal levels at the exhaust, $I_e(\lambda_i)$, were indistinguishable from background, so $I_e(\lambda_i)$ can be approximated by $I_b(\lambda_i)$. Lamp and transmittance spectra (background subtracted) are presented in Figs. 7 and 8 for the resonance and continuum absorption systems, respectively. Prominent NO gamma band regions are labeled in the figures. Absorption features at the (0,0) band are readily evident, but further corrections were necessary to remove position-dependent lamp signal variations and attenuation effects of the exhaust and gas recirculation. These effects are exhibited as overall attenuation at spectral regions away from the (0,0) band absorption feature. A curve fit through spectral regions just above and below the (0,0) band feature served as the base line to quantify (0,0) absorption as illustrated by the "corrected" curve in Figs. 7b and 8b. Thus, the transmittance at the second bandhead of the NO gamma (0,0) band can be read directly from the "corrected" curves.

Previously, spectral bandhead transmittances were determined using pretest lamp reference spectra acquired at each radial position and then corrected for test media attenuation

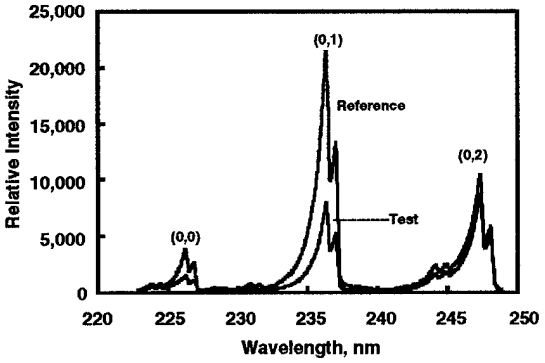

a. Lamp spectra

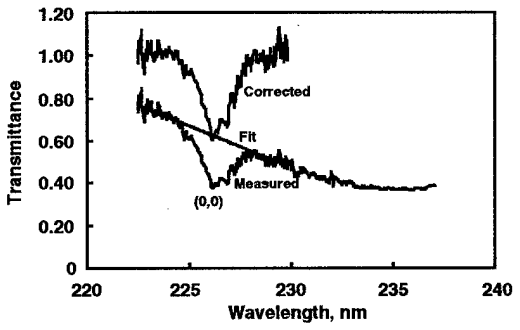

b. Spectral transmittance

Fig. 7. Resonance absorption system spectral data.

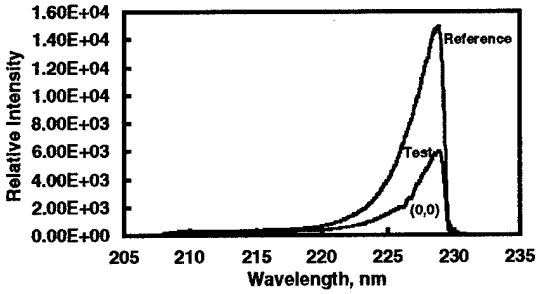

a. Lamp spectra

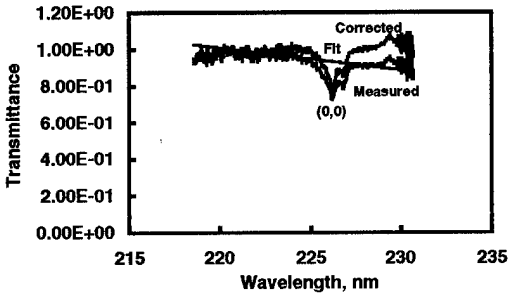

b. Spectral transmittance

Fig. 8. Continuum absorption system spectral data.

effects. Data were reduced both ways and gave equivalent results; i.e., differences in second bandhead transmittances from the two processes were far less than the statistical uncertainties. The purged path allowed an independent measure of lamp reference per data set and all the advantages that go with measuring lamp reference spectra within seconds of acquiring transmission measurements. Statistical uncertainty is discussed later.

Resonance absorption system radial profiles of (0,0) second bandhead transmittance, acquired at the five steady-state engine power settings at 9.1-km altitude, are shown in Fig. 9a. These

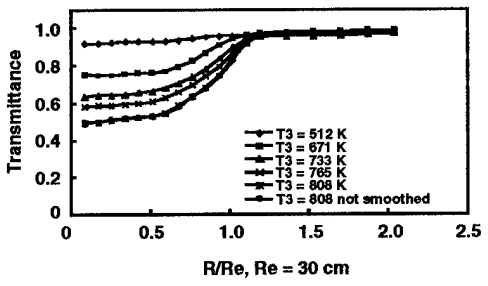

a. Resonance absorption system

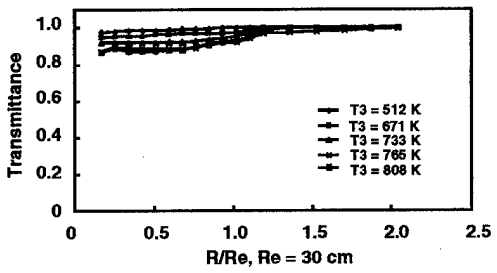

b. Continuum absorption system

Fig. 9. Radial profiles of (0,0) transmittance at 9.1-km altitude.

profiles were smoothed using a linear 3-point smoothing algorithm before insertion into the radial inversion scheme. Representative effects of the smoothing algorithm are illustrated by the smoothed and unsmoothed transmittance profiles in the figure for T3 = 808 K. Although random-like variations were reduced, changes in transmittance values were generally much smaller than statistical measurement uncertainty. Several sets of transmittance profiles acquired at the same steady-state engine condition were extremely repeatable, with smaller variations than statistical measurement uncertainty. The multiple transmittance profiles acquired during a steady-state test condition were averaged before application of the radial inversion scheme.

Continuum absorption system radial profiles of second bandhead (0,0) transmittance, also acquired at the five engine power settings at 9.1-km altitude, are presented in Fig. 9b. Comparing these profiles with resonance absorption profiles of Fig. 9a, it is obvious that the continuum absorption system was less sensitive to equivalent NO densities at the same test conditions. Additionally, continuum absorption was not observed for several low-power engine settings which produced relatively low NO densities. Preliminary results on selected data sets indicate higher uncertainties than results obtained from the resonance absorption data.

The higher-quality and more complete resonance absorption data were analyzed and are reported herein.

ANALYSIS AND RESULTS

The radiative transfer model, [Eq. (1)], incorporated into the onion peel radial inversion scheme was applied to radial transmittance profiles for each steady-state engine test condition. Static temperature and pressure profiles required for the radiative transfer model were inferred from probe and facility measurements and averaged along "homogenous" zones for each LOS optical path. The analysis provides radial NO number density (molecules per volume) profiles. For a more direct comparison to probe sampling measurement profiles, radial NO-UV number density (cm^{-3}) profiles were converted to volumetric fractions (ppmv) using the ideal gas law. Profile comparisons are presented in Figs. 10 - 12 for the same combustor temperature setting, T3 ≈ 733 K, at three different altitudes, 3.1, 9.1, and 12.2 km, respectively. The NO-UV densities tend to be similar in shape to the sampling measurements, but lower by 10 percent for 9.1 and 12.2 km, and about 18 percent for SLS. The stronger deviation might be expected at higher engine power settings for the SLS condition because of the combined effects of greater quantities of NO recirculation in the test cell and pos-

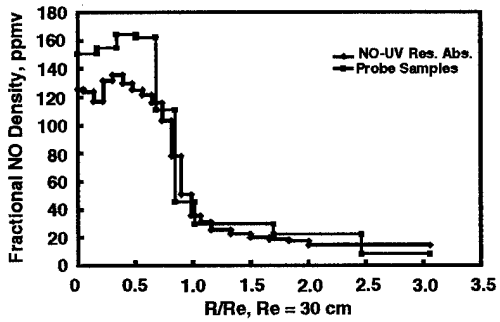

Fig. 10. Resonance absorption and probe sampling radial profiles of NO density for T3 = 733 K and sea-level-static (3-km) altitude.

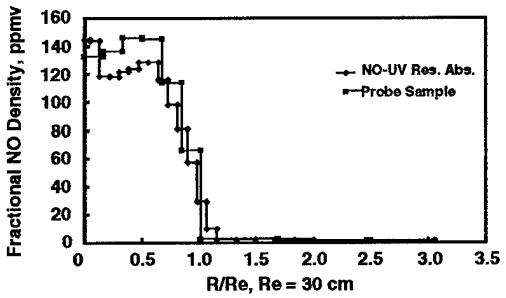

Fig. 11. Resonance absorption and probe sampling radial profiles of NO density for T3 = 733 K and 9.1-km altitude.

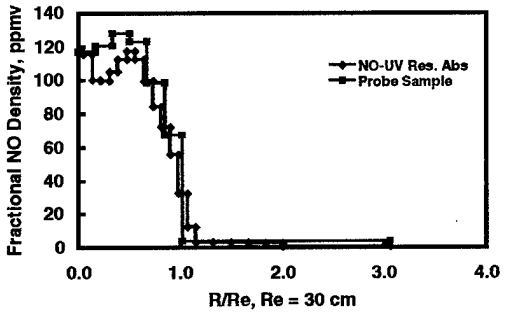

Fig. 12. Resonance absorption and probe sampling radial profiles of NO density for T3 = 733 K and 12.2-km altitude.

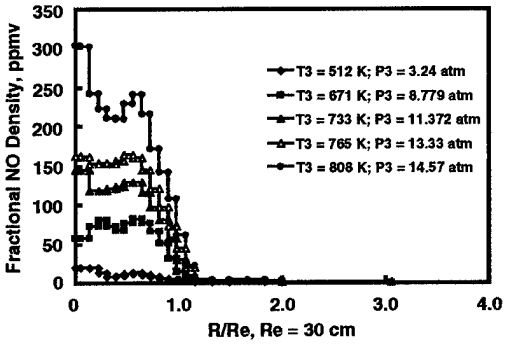

Fig. 13. Resonance absorption radial profiles of NO density for all combustor temperatures at altitude = 9.14 km.

sible non-radial symmetries (especially top to centerline) in the recirculation region. Figure 13 shows NO density profiles for each engine power setting at the 9.14-km altitude.

Direct comparisons of density profiles were limited to the few test conditions for which spatial probe sampling profiles were measured. For comparisons over the full set of test conditions, emission indices were calculated from NO-UV resonance absorption density profiles, aerodynamic flow-field properties derived from the rake data, and fuel flow rates measured by the test facility. An NO emission index EI(NO) using the molecular weight of NO_2 was determined for each engine condition according to

$$EI(NO) = \frac{1000*M_{NO_2}}{N_A*(\text{fuel flowrate})}\left(\sum_j (n_{NO})_j\right)V_{x_j}A_j \quad (3)$$

where N_A is Avagadro's number, and M_{NO_2} is the gram molecular weight of NO_2. The quantities n_{NOj} and Vx_j are zone averaged NO number density and exhaust velocity, respectively, and A_j is the cross-sectional zone area at the measurement axial station. These EI(NO) values are presented in Figs. 14 - 18, and are compared to probe sampling and infrared tunable-diode laser technique results. Measurements from all three measurement systems agree within respective uncertainty bands.

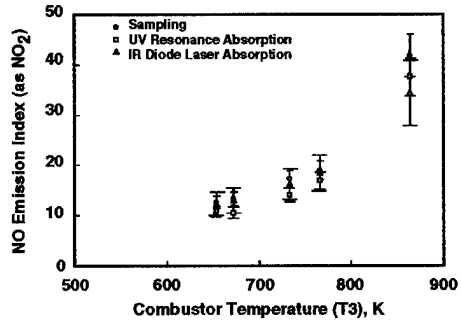

Fig. 14. Comparisons of EI(NO) at simulated sea-level-static condition.

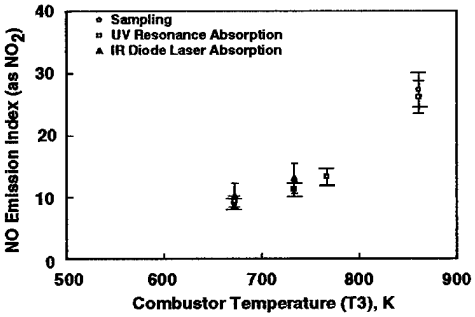

Fig. 15. Comparisons of EI(NO) at 7.6-km altitude.

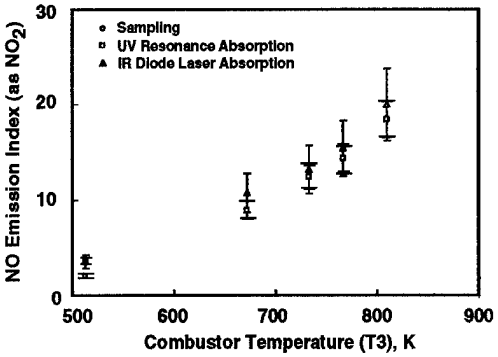

Fig. 16. Comparisons of EI(NO) at 9.1-km altitude.

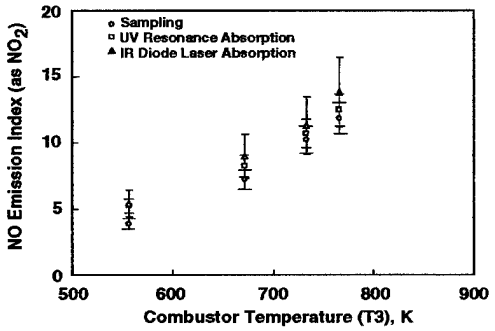

Fig. 17. Comparisons of EI(NO) at 12.2-km altitude.

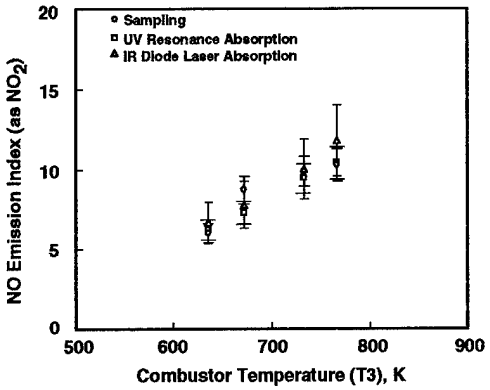

Fig. 18. Comparisons of EI(NO) at 15.2-km altitude.

UV EI(NO) measurements were in good agreement with probe sampling data, matching well within respective uncertainty bands. A contribution of uncertainty not addressed in these comparisons relates to aerodynamic flow-field properties determined from the rake probe data. As mentioned, total temperature and Mach flow-angularity probes were sparsely spaced, providing a coarse definition of property profile gradients. The slow-varying nature of these properties across the exhaust flow field provides confidence in values reported, except near the edge of the plume, where changes are more abrupt and the gradient steepens, especially in velocity. The uncertainty in the position at which the velocity drops abruptly to the ambient static condition outside the plume may be a major contributor to differences in EI reported by sampling and optical techniques.

An engineering statistical analysis process described in Ref. 10 was applied to steady-state test conditions for which several sets of measurements were obtained to establish confidence bands for the NO-UV resonance absorption results. Lamp reference and position-wise lamp transmission spectra were treated as independent measurements with random statistical uncertainty. The variance-covariance matrix developed for a set of profile transmittances accounted for codependency on lamp reference spectra, curve-fit correction factors, and the linear smoothing algorithm. Measurement uncertainty and a matrix of partial derivatives of NO number density with respect to transmittance for each zone of each LOS measurement path produced one-sigma variances for NO number densities at each radial location per set of data. Independently, statistical analyses were performed on these multiple data sets acquired at steady-state engine conditions, treating each set of spatial transmittances as independent measurements with random uncertainty. The resulting uncertainty in NO number density was similar. This tends to validate assumptions used for the lengthy and tedious engineering statistical analysis process[10] required for single data sets obtained for many of the steady-state engine conditions.

The position-wise NO number density uncertainties within the exhaust flow for several test conditions investigated ranged from ± 6 to 18 percent, with the higher uncertainties relating to data at higher combustor temperatures for the simulated sea-level-static condition. Statistical uncertainty on position-wise NO densities determined for the recirculation flow region were on the order of ± 15 to 25 percent. Statistical uncertainty for NO emission indices ranged from ± 7 to 13 percent assuming accurate velocities from the rake data.

For completeness, resonance absorption was also observed at the (0,1) band for a limited number of the higher combustor temperature conditions. NO densities determined from the (0,1) data are consistent with (0,0) results, but with larger uncertainties attributable to a greater sensitivity on static temperature.

SUMMARY AND CONCLUSIONS

NO-UV resonance absorption measurements were performed at all test conditions consisting of several engine power settings at simulated altitudes ranging from sea-level-static to 15.2-km static. At an axial position within 12 cm of the nozzle exit plane, spectral transmission measurements at multiple radial stations across the exhaust plume flow field and surrounding region containing low-level recirculated exhaust gases were radially inverted to provide radial profiles of NO number density. Radial NO number density profiles in units of cubic centimeters were converted to radial profiles of NO concentrations in units of parts per million by volume and, subsequently, to NO emission indices. Radial profiles of static temperature, static pressure, and exhaust flow velocity inferred from probe rake data were utilized for analyses of the optical data.

The NO-UV measurement system proved to be reliable and robust. Measurements were extremely repeatable during steady-state test conditions, also indicating temporal stability of engine steady-state operation and test facility parameters. NO-UV radial concentration profiles agreed well (within uncertainty limits) with probe sampling measurements, both within the exhaust flow field and the surrounding gas recirculation regions. The NO-UV concentrations tended to have lower peak levels within the exhaust plume region. Greater deviations were expected in comparisons of NO emission indices due to the lack of spatial detail defining the velocity gradient near the edge of the plume. However, NO emission indices determined from NO-UV profile concentrations deviated only a few percent from the probe sampling results.

The NO-UV resonance absorption provided redundancy in NO concentration measurements with a technique independent of the extractive sampling system. Agreement among the two techniques gives confidence that the extracted sample reaching the analyzer was indeed representative of the exhaust gases, as well as validating the optical technique over this range of measurement conditions.

Agreement with the single line-of-sight tunable diode laser technique results are gratifying, but analyses of those data relied upon normalized spatial distribution profiles of NO from either the probe sampling or NO resonance absorption profiles. Traversing the TDL beam or directly comparing the TDL NO measurement with a similar TDL CO_2 along the same line of sight, as discussed in Ref. 1, would greatly enhance the utilization of that technique and provide a more meaningful comparison.

REFERENCES

1. Howard, R. P., et al., "Experimental Characterization of Gas Turbine Emissions at Simulated flight Altitude Conditions," AEDC-TR-96-3 (AD-314312), September 1996.

2. Few, J. D., McGregor, W. K., and Glassman, H. N., "Resonance Absorption Measurements of NO Concentration in Combustor Exhausts," AIAA Progress in Astronautics and Aeronautics-Experimental Diagnostics in Gas Phase Combustion Systems, B.T. Zinn, ed., AIAA Press, Princeton, NJ, 1977.

3. Howard, R. P., Dietz, K. L., McGregor, W. K., and Limbaugh, C. C., "Nonintrusive Nitric Oxide Density Measurements in the Effluent of Core-Heated Airstreams," AIAA 21st Fluid Dynamics, Plasma Dynamics and Lasers Conference, AIAA-90-1478, June 18-20, 1990, Seattle, WA.

4. Roberts, W. L., et. al., "Measurement and Prediction of Nitric Oxide Concentration in the HYPULSE Expansion Tube Facility," 18th AIAA Aerospace Ground Testing Conference, June 20-23, 1994, Colorado Springs, CO.

5. Howard, R. P. and Phillips, W. J., "UV Absorption Technique for Monitoring Mobile Source NO Emissions," 86th Annual Meeting & Exhibition, June 14-18, 1993, Denver, CO.

6. "Procedure for the Calculation of Gaseous Emission from Aircraft Turbine Engines," SAE ARP1533, April 30, 1982.

7. Few, J. D. and Lowry, III, H. S., "Reevaluation of Nitric Oxide Concentration in Exhaust of Jet Engines and Combustors," AEDC-TR-80-65 (AD-A103118), August 1981.

8. Davis, M. G, McGregor, W. K., and Few, J. D., "Utilizing the Resonance Line Absorption Technique to Determine the Collisional Broadening Parameters of a Diatomic Molecule: NO γ-Bands as an Example," *Journal of Quantative Spectroscopy and Radiative Transfer*, Vol. 16, No. 12, December 1976, pp. 1109-1118.

9. Chang, A. Y., DiRosa, M. D., and Hanson, R. K., "Temperature Dependance of Collision Broadening and Shift in the NO A←X (0,0) Band in the Presence of Argon and Nitrogen," *Journal of Quantitative Spectroscopy and Radiative Transfer*, Vol. 47, No. 5, pp. 375-390, 1992.

10. Limbaugh, C. C., "An Uncertainty Propagations Analysis for an Infrared Band Model Technique for Combustion Gas Diagnostics,"AEDC-TR-76-155 (AD-A038063), April 1977.

REPORT DOCUMENTATION PAGE

Form Approved
OMB No. 0704-0188

1. AGENCY USE ONLY *(Leave blank)*	2. REPORT DATE	3. REPORT TYPE AND DATES COVERED
	October 20-24, 1997	Technical Society Paper

4. TITLE AND SUBTITLE
UV Absorption Measurements of Nitric Oxide Compared to Probe Sampling Data for Measurements in a Turbine Engine Exhaust at Simulated Altitude Conditions

5. FUNDING NUMBERS

6. AUTHOR(S)
R. P. Howard

7. PERFORMING ORGANIZATION NAME(S) AND ADDRESS(ES)
Sverdrup Technology, Inc., AEDC Group
Arnold Engineering Development Center
Arnold Air Force Base, TN 37389-9013

8. PERFORMING ORGANIZATION REPORT NUMBER

9. SPONSORING/MONITORING AGENCY NAME(S) AND ADDRESS(ES)
Arnold Engineering Development Center/DOT
Air Force Materiel Command
Arnold AFB, TN 37389-9011

NASA Lewis Research Center
21000 Brookpark Road
Cleveland, OH 44135-3191

10. SPONSORING/MONITORING AGENCY REPORT NUMBER
AEDC-TR-96-3

11. SUPPLEMENTARY NOTES
Presented at AGARD 90th Propulsion & Energetics Panel (PEP) "Advanced Non-Intrusive Instrumentation for Propulsion Engines," on October 20-24, 1997 in Brussels, Belgium. Also included as part of AGARD proceedings publication.

12a. DISTRIBUTION AVAILABILITY STATEMENT
Approved for public release; distribution unlimite

12b. DISTRIBUTION CODE
A

13. ABSTRACT *(Maximum 200 words)*
Nitric oxide measurements were conducted in the exhaust of a turbofan engine at simulated altitude conditions in a ground-level test cell using both optical non-intrusive and conventional gas sampling techniques. NO-UV absorption measurements, using both resonance and continuum lamps, were made through several chords of the exhaust flow near the nozzle exit plane as a part of a larger effort to characterize aircraft exhaust constituents over a wide range of steady-state engine operating conditions. This paper describes the NO-UV absorption measurements and compares radial profiles of NO concentrations and emission indices with measurements obtained using conventional gas sampling and tunable diode laser infrared absorption.

14. SUBJECT TERMS
UV-Absorption, NO-UV resonance absorption, turbine emissions, nitric oxide, altitude turbine emissions

15. NUMBER OF PAGES
9

16. PRICE CODE

17. SECURITY CLASSIFICATION OF REPORT	18. SECURITY CLASSIFICATION OF THIS PAGE	19. SECURITY CLASSIFICATION OF ABSTRACT	20. LIMITATION OF ABSTRACT
UNCLASSIFIED	UNCLASSIFIED	UNCLASSIFIED	UL